International Journal of Computational and Theoretical Chemistry
2026, Vol. 14, No. 1, pp. 15–33
https://doi.org/10.11648/j.ijctc.20261401.12

SciencePG
Science Publishing Group

Research Article

A Computational Investigation of Spectroscopic, Molecular, and Electrostatic Properties of the Schiff Base Molecules via DFT

Muhammad Javid[1, *], Ifra Shahzadi[2], Farah Jamil[3], Sabahat Asghar[2], Muhammad Sajid Abbas[4], Ihsan Maseeh[5], Muhammad Hasnain[6], Muhammad Zohaib Sabir[7]

[1]Department of Chemistry, University of Agriculture Faisalabad, Punjab, Pakistan

[2]Institute of Chemistry, Khwaja Fareed University of Engineering and Information Technology, Rahim Yar Khan, Punjab, Pakistan

[3]Department of Applied Chemistry, Government College University Faisalabad, Punjab, Pakistan

[4]Department of Physics, University of Agriculture Faisalabad, Punjab, Pakistan

[5]Institute of Chemistry, The Islamia University of Bahawalpur, Punjab, Pakistan

[6]Department of Chemistry, University of Agriculture Faisalabad, Punjab, Pakistan

[7]Department of Chemistry, King Mongkut's Institute of Technology Ladkrabang, Bangkok, Thailand

Abstract

This theoretical work give a comprehensive properties of a Schiff base compound that is formed when amines and ketone or aldehyde are combined. The investigated Schiff base compounds were designed by combining primary amines with ketones or aldehydes. The spectroscopic characteristics, molecular structure, electrostatic potential maps, and other molecular properties of these compounds had been computed at the B3LYP Functional with a 6-311G(d,p) basic set. The optimization and transition states of the molecules were analyzed by applying the B3LYP Functional with a 6-31G(d,p) basic set, based on density functional theory (DFT) and time-dependent density functional theory (TD-DFT) for ground-state and excited-state calculations, respectively. We had also determine the band length and band angles of the designed molecules. Several computational software packages was used to study the spectroscopic, electronics, and molecular characteristics of explore Schiff base compounds. The molecules were designed in GaussView5 and optimized in Gaussian 09. PyMolyze and Origin6.0 software were used to perform the density of state (DOS) analysis & to draw the absorption spectra of probe molecules. TDM analysis were conducted to determine the charge distribution in the investigated molecules using Multiwfn3.7 and VMD1.9.1 software. Correlation statistical models were employed to interpret the statistical data. The docking results of the designed molecules were compared with antibacterial standards, and we expect these results to show greater efficiency than the reference molecules. Additionally, the antitumor and antibacterial characteristics of a designed molecule were compared with those of the reference molecules.

*Correspondence: Muhammad Javid (javidkhanchemist@gmail.com)

Received: 3 June 2026; **Accepted:** 16 June 2026; **Published:** 8 July 2026

Keywords

DFT, B3LYP, Schiff Base, Optimization, Transition States, Spectroscopic

1. Introduction

Schiff base is a molecule that carrying a functional group known as an azomethine (RHC=NH) group, which is made from combination of a primary amine with a ketone. The resulting imine linkage (C=NH) is refer as a Schiff base. Schiff base have the general structure formula R1HC=NR′, where R and R' can be various organic groups or hydrogen atoms, and R′2 is usually an organic group [1]. The azomethine imine group, represented by the (C=N) bond, is responsible for the characteristic properties of Schiff base. In Schiff base molecules, the two main functional groups that are of particular importance are the amino (NH_2) group and the imine (C=N) group [2]. These functional groups play vast roles in the properties and reactivity of Schiff base molecules. Schiff base and their derivatives can tolerate various functional groups, allowing for the introduction of different substituents [3]. This imine (C=N) double bond is central to the structure of Schiff bases. The formation of a carbon-nitrogen double bond in a Schiff base molecules involves the combination between a ketone and a primary amine [4]. The tetrahedral intermediate formed in the previous step is protonated by an acid or by an excess of the amine itself. The carbon and nitrogen double bond provides stability to Schiff base molecules [5]. It exhibits partial double bond character due to resonance, leading to a relatively stable structure molecules. The strength of the imine (C=N) bond in Schiff base can alter base on many factors [6], consist the nature of the substituents at the nitrogen and carbon atoms, as well as the surrounding environment. Generally, the (C=N) bond in Schiff bases is relatively stable under normal conditions. The stability of the (C=N) bond is influenced by steric effects and electronic and of the substituents on the carbon and nitrogen atoms [7]. Electron-withdrawing groups bonded to either the C or N atom can stabilize the (C=N) bond by withdrawing electron density from the bond, thus increasing its strength. The surrounding environment can also affect the firmness of the O=N bond in Schiff base. The presence of other functional groups or neighboring substituents can influence the solidity of (C=N) bond through steric interactions. Bulky substituents near the C=N bond can hinder rotation around the bond and increase its stability [8].

The (C=N) double bond facilitate Schiff base molecules to undergo tautomeric isomerization, wherein the proton can migrate between the nitrogen and carbon atoms. This isomerization between the imine and enamine forms is important in the reactivity and catalytic properties of Schiff base molecules [9]. Isomerization can occur due to the appearance of a C=N bond in Schiff base. Schiff base with a double bond in the imine group exhibit cis-trans isomerism. The isomerization between Cis-Trans forms can occur under certain conditions and affect the properties and reactivity [10]. The C=N bond in Schiff base is a double bond, and it exhibits geometric isomerism. The two possible geometric isomers are the E-isomer (Tran's configuration) and the Z-isomer (cis configuration). Isomerization of Schiff bases can occur through the interconversion between the E and Z isomers [11]. Isomerization of Schiff bases due to the (C=N) bond can have important implications in their reactivity, stability, and biological activity. The different geometric isomers can exhibit distinct chemical properties and exhibit different interactions with other molecules. Therefore, understanding the isomerization behavior of Schiff base is crucial in various fields, including organic synthesis, coordination chemistry, and medicinal chemistry [12].

The reactivity of the (C=N) double bond contributes to versatility of Schiff bases in organic syntheses and medicinal science [13]. This makes the imine nitrogen atom a potential coordination site for various metal ions. The coordination of the imine group can occur through the nitrogen atom, which donates its bond pair of electrons to the metal center [14]. The coordination of the imine group in Schiff base can have several consequences. Schiff base ligands often show chelating behavior, where the imine nitrogen and other donor atoms /ions, forming a stable chelate ring structure [15]. This chelation can enhance the stability of the complex [16]. The coordination of the imine group can influence the properties of the resulting Schiff base complex. The steric and electronic characteristic of the imine ligand can affect the coordination geometry, electronic structure, and reactivity of the complex [17]. The coordination of the imine group can occur through the nitrogen atom, which donates its bond pair of electrons to the metal center. The coordination of the imine group in Schiff base molecules can have several consequences [18]. Schiff base ligands often exhibit chelating behavior, where the imine nitrogen and other donor atoms /ions, forming a stable chelate ring structure [19].

The azomethine bond becomes polarized because nitrogen has a greater electronegative charge than carbon. The electronegative group on the azomethine group decreases polarization and enhances the covalent nature of the double bond by pushing the negative charges on the nitrogen atom toward the carbon [20]. Due to the nitrogen atom's lone pairs of electrons and the double bond's potential to donate electrons, all compounds of schiff base containing an azomethine group exhibit

significant characteristics [21].

The amino group in Schiff base can participate in redox reactions [22]. It can undergo oxidation or reduction processes, either directly or indirectly through the metal center in Schiff base complexes. These redox reactions can be utilized in various applications, including catalysis and organic synthesis [23]. The amino group in Schiff bases can undergo substitution reactions with suitable reagents. The amino group is capable of forming hydrogen bonds with other molecule or functional groups [24]. This hydrogen bonding ability can influence the properties, solubility, and intermolecular interactions of Schiff base. The amino group contains a nitrogen atom with a lone pair of electrons, which can interact with hydrogen atoms attached to electronegative atoms [25]. Hydrogen bonding in Schiff base involving the amino group typically occurs when the nitrogen lone pair interacts. The making of hydrogen bonds between the amino group and other functional group in Schiff base can have important implications for their chemical and physical properties [26]. These interactions can influence molecular conformation, solubility, stability, and even biological activity in certain case. It's valuable to note that the specific hydrogen bonding interactions in a Schiff base can vary depending on the structure and neighboring groups present in the molecule [27]. The presence of multiple function groups and the overall molecular geometry play significant roles in determining the specific hydrogen bonding patterns. Therefore, it's advisable to consider the specific Schiff base structure to understand the precise hydrogen bonding interactions involving the amino group [28].

The amino group is a basic functional group, which have ability to accept protons (have a vacant orbital) by donating a pair of electron and act as a base [29]. This basicity is important in determining the overall acidity/basicity of Schiff base-containing compounds [30]. The C=N group and the NH_2 group in Schiff base contribute to their formation, stability, reactivity, coordination properties, and intermolecular interactions [31]. These functional groups provide Schiff base with unique characteristics and versatility, making them valuable compounds in various areas of chemistry [32]. The basicity of an amino group in a Schiff base can vary depending on the specific structure of the Schiff base molecules. The conjugation in Schiff base involves the delocalization of electrons between the oxygen atom of the amino group and the carbine atom of the amine group [33]. Electron-withdrawing group's link to the imine hydrogen can further reduce the basicity, while electron-donating groups can increase it [34]. The basicity of the amino group in a Schiff base is generally lower compared to a primary amine due to the presence of conjugation, but it can be influenced by the specific substituents and structural features of the Schiff base. The basicity will significantly diminish when the s character increases in hybridization [35].

2. Materials and Methods

Computational Details

The Density Functional Theory has been widely used in the theoretical field for evaluating the charge transmission, morphology, and electrical and photophysical characteristics of newly designed materials, as well as their best outcomes associated with the basis sets used in the calculations. All computational calculations are performed using the Gaussian 09 software [36]. Different basis sets possess different parameters in the calculation, like ionization potentials (IP), electron affinity (EA), molecular orbitals, hole/electron-donating power, etc. The B3LYP basis set is considered a modest size and commonly used for medium-sized organic molecules. The benchmarking was also considered for the selection of the function and basis set. The first four functions, B3LYP, CAM-B3LYP, MPW1PW91, and ωB97XD, were employed in the gaseous and solvent (DCM) phases with a 6-31 g(d,p) basis set using the solvation model, the Integrated Equation Formalism Polarizable Continuum Model (IEFPCM). B3LYP showed more promising and closer UV-Vis spectrum values (531 nm) to the experimental absorption value (582 nm). Additionally, benchmarking with def2-TZVP and M06-2 × was performed, and results are included in the Supporting Information. The most promising function and basis set combination in terms of PDI molecule optimization and computational cost, is B3LYP 6-31 g(d,p). So, the molecular structures have been globally optimized with B3LYP/ 6-31 g(d,p) for identifying the equilibrium molecular geometry. Similarly, electron density difference map (EDDM) analysis, nature bond orbital (NBO) investigations and interaction (IE), vertical ionization energies (VIE) are estimated through the same computational method. Further, the density of states (DOS) analysis was carried out through PyMolyze software and UV-visible absorption spectra were demonstrated through Microsoft origin 2018 software, and Multiwfn[37]. Gaussian software is an important and wonderful application of computational chemistry. It is extensively used in different fields of research like Physics, chemistry. Biochemistry, and chemical engineering [38]. It also helps a lot to critically analyze the different molecules and molecular reactions. Gaussian software is highly essential and significant in determining the variety of different spectra including IR, UV/Vis, NMR and RAMAN, etc. The Gaussian view is a graphical user interface which is an essential feature of Gaussian software [39]. The Gaussian 09 tool has been utilized to optimize the molecule' geometry initially. Rather than optimal system the resulting data generally provide facts on the electrical aspects [40]. Latest energy as well as optimization perform a fundamental role in preliminary estimations throughout this technique. From of its optimized form the angles of bond as well as length of bond were measured [41].

3. Result and Discussion

In this research work, we have designed three molecules named as SL1, SL2, and SL3. Optimization geometries of designed molecules were calculated and analyzed computationally to evaluate their structural and spectroscopic properties

by DFT at B3LYP method at 6-311+G(d,p) bases set. In this study, different methods were applied to find out the best organic semiconductor molecule for the efficient working of organic thin film transistors such as B3P86, B3W91, CAM/B3LYP, M06 and B3LYP with 6-31G(d,p) basis set [42]. Different basis set has been applied such as 6- 311G(d,p), 6-310(d,p).6-310 (d) and 6-311G(d,p). The reliable results were obtained by using B3LYP with 6-31G(d,p). Our research aim was to find out the molecules with the lowest Egap between HOMO and LUMO energy levels and low value of reorganization energy which was obtained by apply the B3LYP method with a 6-31G(d,p) basis set. As previously mentioned, to attain the best results the E_{gap} between HOMO and LUMO energy levels should be the very small [43]. The aim is to increase the efficient power in such molecules which improve charge carrier properties. In our work, we kept the same scheme for a newly designed molecule that is used in the reference but added substitution to make more efficient results for investigated molecules and to gain the desired results [44]. Another aim is to increase the conjugation so that the electron mobility can be increased enhancing the electron transfer rate. In reference molecule, two fragments have used the names as SL1, SL2, and SL3.

3.1. Scheme of Study

We have designed the structure scheming of the considered Schiff base molecules in the framework of TD-DFT. This examination was accomplished with the point of directing the next formation towards Schiff base molecules progressively as anticancer drugs.

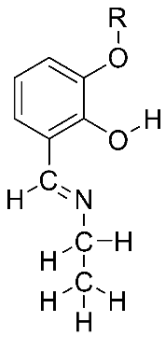

Figure 1. *Designed Schiff base investigated molecule.*

The above designed molecule (Figure 1), we have examined the impact of the various structures of the Schiff base molecules on the optoelectronic properties. A surface molecules of Schiff base has been investigated by introducing different group R1 is OCH3, R2 is OH, and R3 is Cl replace by R1, R2, and R3 is a position. In SL3, a methoxy group (-OCH_3) attached at R of the first Schiff base. In this research work, to achieve the lower energy gap an appropriate strategy of the designed molecules. We have investigated different three molecules of Schiff base name as SL1, SL2, and SL3 (Figure 2) which are substituted with the different functional group.

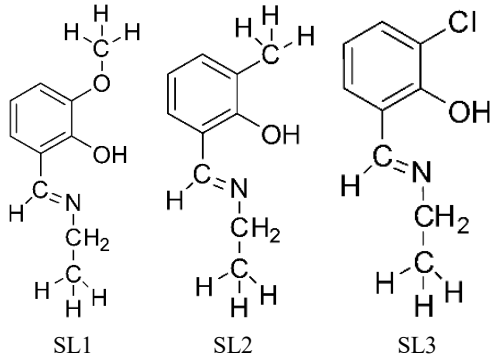

Figure 2. *(SL1) 2-((ethylamino) methyl)-6-methoxyphenol, (SL2) 2-((ethylamino) methyl)-6-methylphenol, (SL3) 2-((ethylamino) methyl)-6-chlorophenol.*

3.2. Optimized Structures

The structures of the designed molecules SL1, SL2, and SL3 were obtained after optimization using Gaussian09 to determine the most stable configuration found in nature. The optimized structures hold significant importance due to their stability. In computational chemistry, the process of energy minimization aims to find a molecular arrangement where every atom is stationary, and the force between atoms is nearly zero [45]. The optimized geometry of these substituted molecules exhibit a planar configuration, as shown (Figure 3) in the accompanying Figure. For the investigated molecules, bond angles were calculated at the substituted positions of the Schiff base molecules to assess their electronegativity. Electronegativity is inversely related to bond lengths, and as bond length increases, bond angles decrease [46]. Although the numbering of elements varies among the investigated molecules due to structural changes, the bond lengths and bond angles at corresponding positions remain consistent regardless of the different numbering schemes.

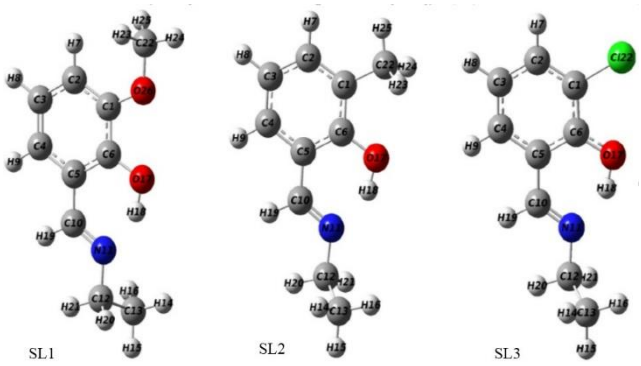

OPT. of SL1 OPT. of SL2 OPT. of SL3

Figure 3. *Ground state optimized structures of designed molecules.*

3.3. IR Spectroscopic Analysis

IR spectroscopy, the spectra of the designed molecules were calculated to investigate their shapes. Nine high intensities peaks have identified for each designed molecule. The infra-red spectra of the designed Schiff base has generally similar to each other as shown in Figure 4. The Schiff base molecules SL1 and SL2 exhibited peaks at approximately 689.7 cm^{-1} due to the C-C stretching vibration [47]. A notable characteristic of the designed Schiff bases was the -C=N- bond, with peak number seven corresponding to the C=N stretching vibration. The stretching frequencies for the SL1, SL2, and SL3 molecules were 1705, 1706, and 1809.2 cm^{-1}, respectively. When this factor is applied to the three values mentioned above, the calculated frequencies are 1623.9, 1624.3, and 1625.2 cm^{-1}, respectively [48].

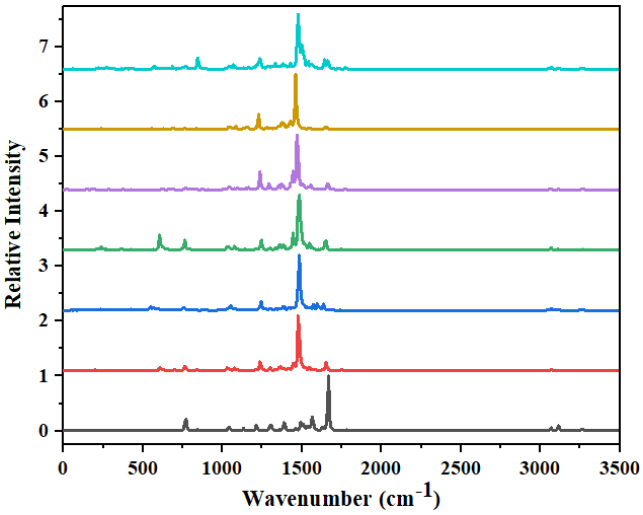

Figure 4. *IR Spectrum of SL1, SL2, and SL3.*

Table 1. *The vibrational modes, frequencies, and intensities of specific bonds in studied complexes were detected by IR graphs of SL1, SL2, and SL3.*

Molecules	Bonds	Vibrational Modes	Frequency (cm^{-1})	Intensity
SL	C—N	Scissoring	809.06	600.34
	H—N	Symmetrical	1204.39	300
	O—N	Symmetrical	1425.63	3500
SL1	H—O—N	Scissoring	610.05	1521.62
	H—N	Scissoring	809.44	964.23
	C—N	Scissoring	825.42	703.75
	O—N	Symmetrical	1063.32	589.39
	N—C—O	Anti-Symmetrical	1144.25	2813.24
	O—N—O	Anti-Symmetrical	1332.40	1717.22
	N—C—N	Anti-Symmetrical	1397.71	2864.40
	C—N—N	Anti-Symmetrical	1421.33	3423.06
	N—C—H	Anti-Symmetrical	1439.72	859.32
	H—N—O	Anti-Symmetrical	1631.41	1146.36
SL2	O—C—H	Symmetrical	395.88	1308.31
	N—O—H	Symmetrical	611.14	1267.08
	H—N—C	Symmetrical	822.71	1335.77
	N—O—H	Anti-Symmetrical	887.12	843.42
	H—N—O	Anti-Symmetrical	1137.45	2965.11
	H—N—N	Anti-Symmetrical	1388.37	4391.08
	N—C—N	Anti-Symmetrical	1412.25	5636.42
SL3	Cl—O—H	Rocking	420.27	1041.28
	O—C -O	Anti-Symmetrical	578.42	1147.82

Molecules	Bonds	Vibrational Modes	Frequency (cm^{-1})	Intensity
	H—O -H	Symmetrical	613.47	1080.07
	H—C—N	Scissoring	1126.47	4517.31
	C—N—Cl	Anti-Symmetrical	1400.46	5476.00
	N—C -N	Anti-Symmetrical	1416.62	3148.02

The vibrational analysis plays a vital role in illuminating the specific molecular structure and associated vibrational modes of the target molecule. This investigation encompassed an examination of the prominent stretching frequencies linked to key bonds, such as O-H, C-O, C=C, N-H, C-H, and N-O, within the IR spectra of SL1, SL2, and the SL3. In the case of B303, the O-H bond exhibited a stretching vibration at 793.4 cm^{-1}, but within the complex, it man- infested a noticeable red shift, reaching 803.91 cm, accompanied by a rocking vibration mode. Similarly, for H-O bonds, we observed an asymmetrical stretching frequency of 1353.73 cm^{-1}, while the complex displayed a notable blue shift, registering at 1328.78 cm^{-1}, In the SL, the N-H bond showcased a twisting vibration mode to 1288.97 cm^{-1} and in the complex, the frequency shifted to 1338.93 cm^{-1}, maintaining the same vibration mode. As for the C-H bond, it presented a wagging vibrational mode in SL, while in the complex, the vibrational mode remained unchanged, but the frequency experienced a red-shift, transitioning from 1288.65 cm^{-1} to 1338.79 cm^{-1}, briefly summarization in the Table 1.

3.4. NMR Analysis

Raman spectroscopy is an analytical tool which used to determined electronic structure and environment of atom within molecules. The compute ^{1}HNMR and ^{13}CNMR spectra of designed molecules SL1, SL2, and SL3 are present in the given Table 2. TMS was used as a stander to calculate the chemical shifts values.

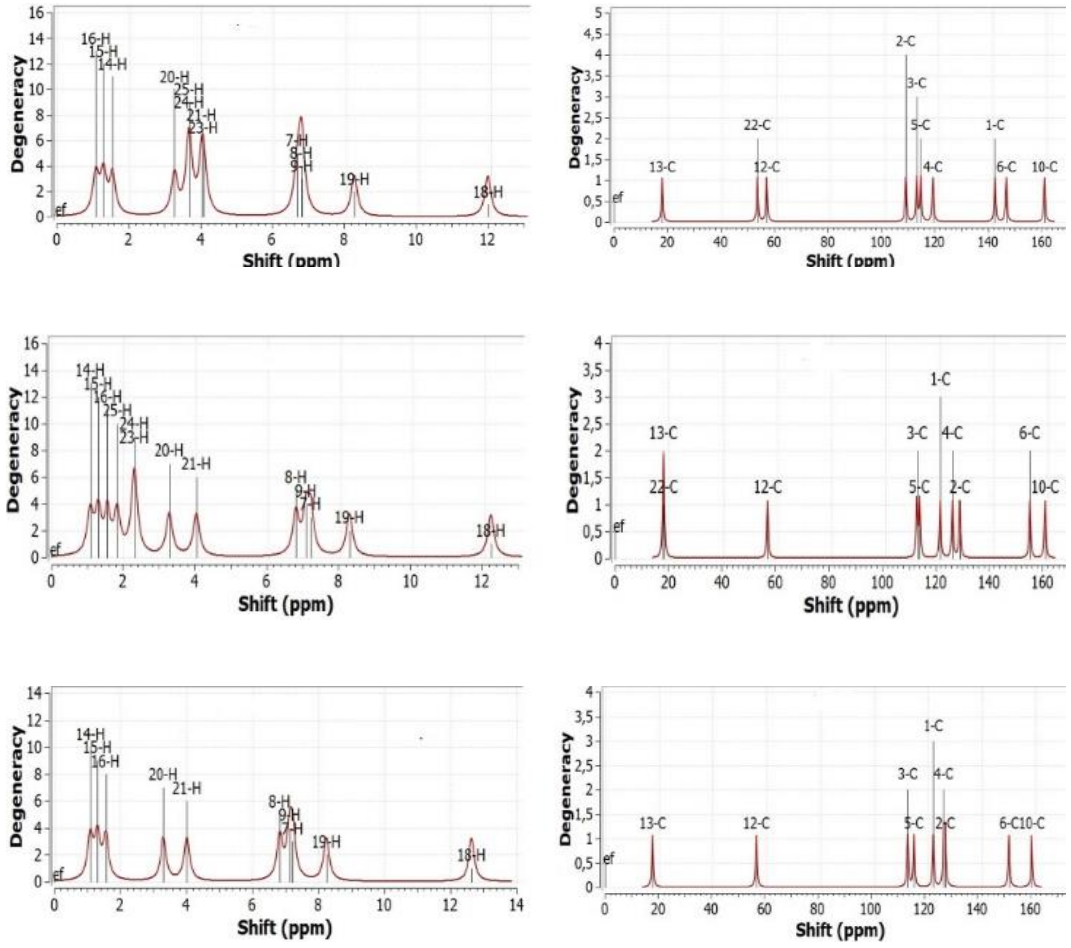

Figure 5. NMR peaks of SL1, SL2, and SL3.

Table 2. *Calculated values of Raman graphs of SL1, SL2, and SL3.*

Molecules	Bonds	Vibrational Modes	Frequency	Raman	Intensity
SL	C—N—H	Scissoring	327.13	5.2388	1.3
	N—C—N	Scissoring	380.49	7.7635	1.2
	H—N—H	Scissoring	562.75	0.0346	4.4
	C—O—N	Wagging	754.41	2.3969	0.4
	H—N—C	Scissoring	807.17	3.6844	0.3
	N—C—H	Wagging	881.15	13.1493	1
	C—C—N	Symmetric	1051.63	0.9426	0.2
	H—N—H	Anti-Symmetric	1183.52	2.3888	0.4
	H—N—C	Anti-Symmetric	1318.24	2.7109	0.2
	C—N—BH	Symmetric	1447.19	1.3304	0.2
SL1	O—N—O	Twisting	31.98	1.2865	0.1
	H—O—C	Scissoring	300.87	5.9279	0.3
	C—N—H	Scissoring	345.00	6.3461	0.4
	N—C—N	Scissoring	384.16	3.7635	0.2
	O—C—O	Anti-Symmetric	567.28	5.1622	0.4
	C—N—H	Twisting	631.71	18.5154	1.1
	B—Li—O	Symmetric	708.17	19.5818	1.2
	N—O—N	Symmetric	873.28	12.684	0.6
	O—N—O	Symmetric	1063.32	25.4996	1.5
	H—N—C	Anti-Symmetric	1318.32	3.7423	0.2
	N—N—O	Anti-Symmetric	1417.23	4.1945	0.2
	H—N—O	Anti-Symmetric	1631.41	8.7024	0.5
SL2	H—N—O	Twisting	19.41	2.1398	0.2
	O—N—H	Scissoring	284.95	4.8997	0.4
	N—O—H	Wagging	308.07	0.5315	0.4
	H—O—C	Symmetric	445.85	4.9158	0.4
	C—N—O	Anti-Symmetric	577.36	28.8333	2.3
	C—N—N	Scissoring	789.73	12.5613	0.9
	H—C—N	Wagging	867.20	15.5730	1.2
	O—N—C	Symmetric	1098.43	44.5076	3.4
	C—O—H	Anti-Symmetric	1290.31	8.0811	0.7
	O—N—C	Anti-Symmetric	1351.23	1.4670	0.3
	H—C—N	Anti-Symmetric	1451.62	7.6134	0.7
	O—N—C	Anti-Symmetric	1611.33	15.2449	1.3
SL3	C—O—C	Scissoring	303.21	4.4150	0.3
	N—O—H	Wagging	333.96	4.4512	0.3
	H—O—Cl	Anti-Symmetric	455.99	3.2037	0.2

Molecules	Bonds	Vibrational Modes	Frequency	Raman	Intensity
	N—O—C	Anti-Symmetric	563.97	8.6161	0.6
	Cl—N—C	Wagging	632.99	13.8687	0.7
	H—O—N	Scissoring	704.58	17.8445	1.1
	N—C—H	Anti-Symmetric	761.52	0.5719	0.2
	N—C—Cl	Scissoring	803.12	1.9640	0.1
	Cl—O—N	Scissoring	820.29	2.4146	0.2
	N—N—C	Scissoring	872.21	13.2304	0.9
	C—N—Cl	Anti-Symmetric	885.06	7.1286	0.5
	O—N—O	Symmetric	1097.90	22.6627	1.4
	N—O—N	Anti-Symmetric	1319.69	3.8103	0.2
	O—N—O	Anti-Symmetric	1350.48	2.8253	0.2
	N—C—N	Anti-Symmetric	1418.41	1.4583	0.3
	Cl—N—N	Anti-Symmetric	1449.32	2.7903	0.2
	O—N—H	Anti-Symmetric	1613.39	10.2655	0.7

The Raman spectra in (Figure 5) depict the vibrational characteristics of SL1, SL2 and SL3. Specifically, we measured the vibrational frequencies associated with certain bond stretching modes in these molecules. In SL1, during the symmetrical stretching mode, we observed a frequency of 3736.60 cm^{-1} for the O-H bond [49]. Conversely, in the SL2, the bond exhibited a red shift having a frequency of 3740.75 cm^{-1}. For the C=C bond, we observed a frequency of 1674 cm^{-1}. In SL2, the bond exhibited a blue shift during the symmetric stretching vibration in SL3, resulting in a decrease in frequency to 1656.72 cm^{-1} [50]. However, in the SL1 carrier, the C=O bond exhibited a symmetrical stretching mode having a frequency of 540.81 cm^{-1} and for SL2, a blue shift occurred in the bond, resulting in a cm frequency of 534.96 cm^{-1}. The C-H bond shows rocking vibration at 2680.15 cm^{-1} and within the complex, it exhibited a red shift by changing the vibrational mode into symmetrical stretching, its frequency increases to 2692.7 cm^{-1} [51]. Summary of the frequency values of all these peaks in the provided (Table 2).

3.5. Frontier Molecular Orbitals (FMOs) Analysis

To distinguish electronic and NLO properties of the examined molecule, frontier molecular orbitals (FMOs) were determined. The sketches of FMOs were used to analyze the optoelectronic properties of the molecules [52], as shown in the Figure 6. The structure of a molecule obtained after optimization is the most stable form found in nature; hence, the optimized structure holds significant importance. The FMOs of the investigated molecules were characterized, and the distribution of LUMO and HOMO energies for the substituted Schiff base molecules was analyzed [53]. The distribution patterns of the frontier molecular orbitals extend across the entire molecules. The highest occupied molecular orbitals are typically located on the EDP of the functional groups, while the lowest unoccupied molecular orbitals (LUMOs) are located in the EWP [54].

Table 3. *Energy gap values.*

Compounds	EHOMO	ELUMO	Energy gap (E g)
SL1	-0.1475ev	-0.1247eV	0.0228eV
SL2	-0.1329eV	-0.0724eV	0.2063eV
SL3	-0.1153eV	-0.1310eV	0.0157eV

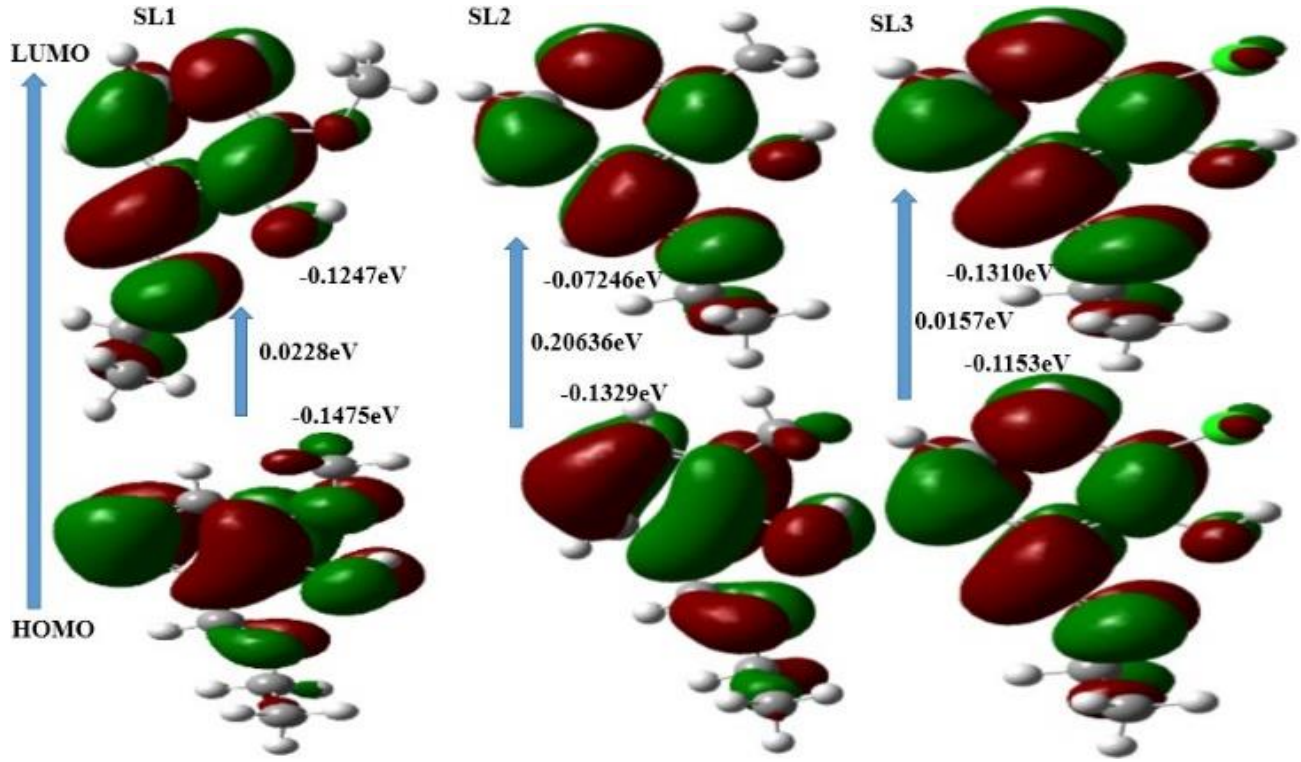

Figure 6. HOMO and LUMO of SL1, SL2, and SL3 Molecule.

3.6. Molecular Electrostatic Potential (MEPs) Analysis

The concept of electrostatic potential serves as a valuable tool in comprehending the arrangement of molecules on an intermolecular level [55]. Visual representations, such as ESP energy maps or molecule electric potential surface, vividly depict the spatial distribution of charges within molecules. Essentially, electrostatic potential energy quantifies the strength of nearby charges, nuclei, and electrons at a specific position [56]. Typically, analysis involving molecular electrostatic potential elucidates the three-dimensional charge distribution of the molecules under investigation. In MEP plots, distinct colors and varying values are assigned to different regions on the surface. The ascending and descending order of MEP is as follows: red < yellow < green < blue < pink < white [57]. In the map, the red and yellow regions represent negative molecular electrostatic potential, indicating electrophilic reactivity. The white region corresponds to positive electrostatic potential, while the blue region signifies zero electrostatic potential within the designed molecules [58]. Designed molecules' separate donor units each contain positive charges, while the middle component is neutral (green color). However, the center of the molecule is dominated by the colour red. Figure 7 indicates that the acceptor of the newly developed compound SL3 has more lone pairs than the other designed molecule, it has a more negative charge distribution, whereas the end of the reference molecule SL has smaller blue patterns.

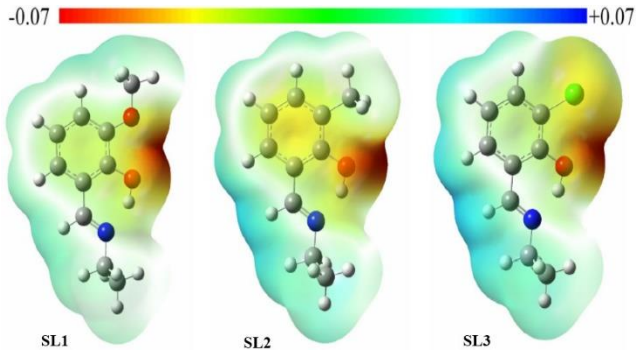

Figure 7. Electrostatic potential maps of the designed molecules.

The calculated MEP value of the designed molecules, it can be observed that the negative regions in the molecules are located around the oxygen atom, while the positive regions are found around the hydrogen atom attached to the nitrogen atom [59]. The overall surface areas for the compounds are as follows: SL1 is 427.77 Å ³, SL2 is 401.62 Å ³, and SL3 is 359.68 Å ³. The electrostatic potential ranges for these compounds are: SL1 from -43.48 kcal/mol to 54.92 kcal/mol, SL2 from -39.41 kcal/mol to 49.00 kcal/mol, and SL3 from -32.86 kcal/mol to 50.80 kcal/mol MEPs surfaces visually represent the 3-D distribution of charges across a molecule, allowing us to identify regions of high and low potential [60]. These surfaces are useful for predicting the presence of electronic moieties on a molecule's surface [61].

3.7. Density of States Analysis

DOS analysis described different energy levels available for the number of state for electrons. A higher values of DOS show a considerable availability of number of states whereas a lower values of DOS indicates the availability of the minimum number of state for occupation [62]. The density of state (DOS) is simply the distinct condition that electrons are allowed to dominate at a given energy level. This function defines bulk parameters and other transformation phenomena of substances [63]. The calculations of DOS may be used to fine the general distribution of states by using the function of energy and in semi-conductors it also helps in interpreting the spacing between different energy bands (Figure 8). Density of state provides the analyses of the percentage contribution of each fragment of the designed molecules through PDOS and TDOS [64]. Density of state of the investigated molecules have been calculated at B3LYP/LANL2DZ level. PyMolyze 2.0 was used for graphical presentation of the molecules.

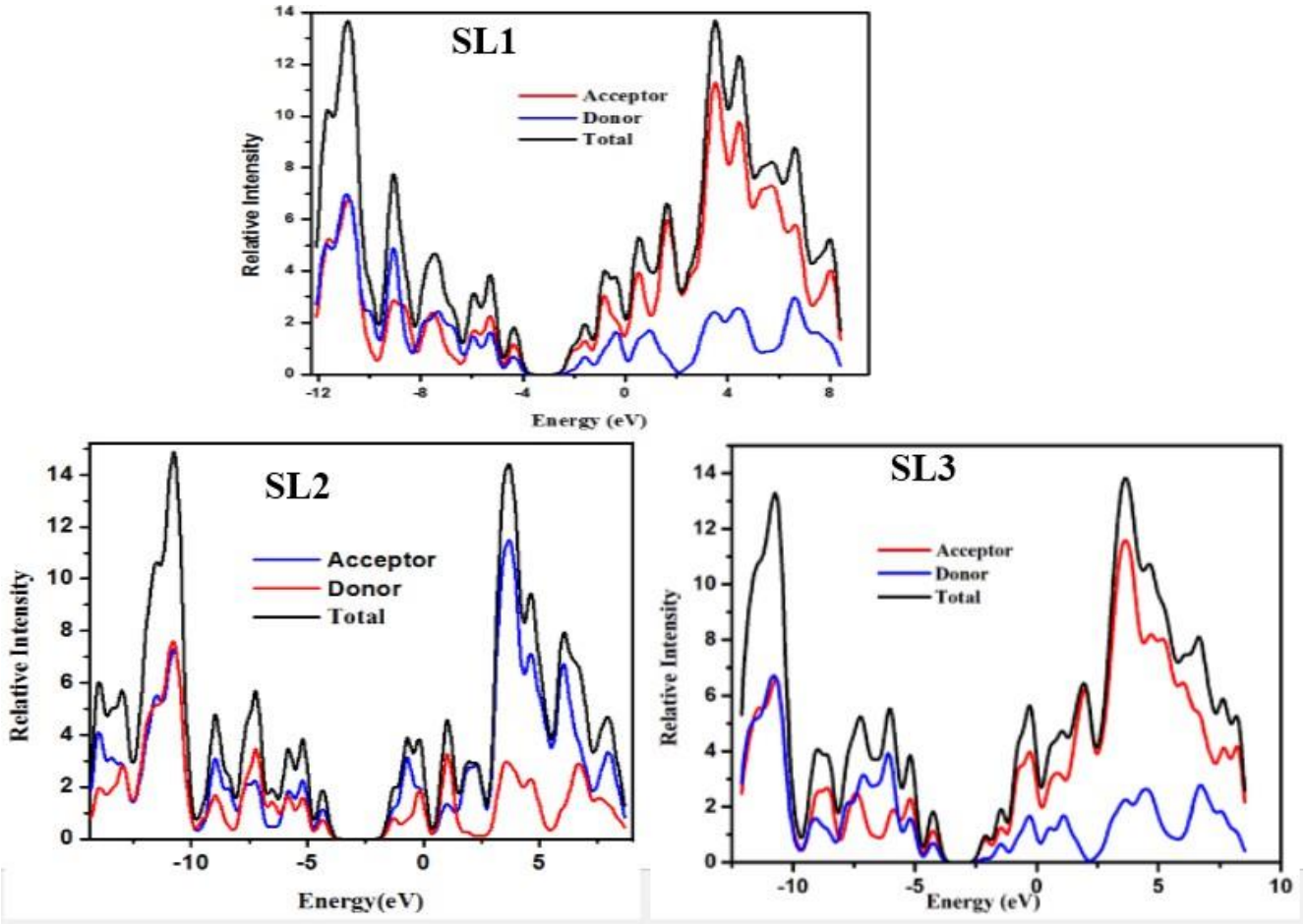

Figure 8. Density of state of SL1, SL2, and SL3 molecules.

Table 4. The percentage contribution of fragments SL1 Molecule.

Energy level	Fragment 1	Fragment 2	Fragment 3
HOMO	61	36	2
HOMO-1	5	92	0
HOMO-2	7	90	1
HOMO-3	54	91	0
HOMO-4	8	93	3
LUMO	85	11	41
LUMO+1	57	3	19
LUMO+2	79	2	13
LUMO+3	75	23	11
LUMO+4	76	8	12

SL1 Molecule

Table 5. *The percentage contribution of fragments SL2 molecule.*

Energy level	Fragment 1	Fragment 2	Fragment 3
HOMO	58	38	1
HOMO-1	8	93	0
HOMO-2	86	91	0
HOMO-3	57	46	1
HOMO-4	79	41	1
LUMO	75	09	4
LUMO+1	80	1	54
LUMO+2	74	2	59
LUMO+3	72	1	20
LUMO+4	78	26	9

Table 6. *The percentage contribution of fragments SL3 molecule.*

Energy level	Fragment 1	Fragment 2	Fragment 3
HOMO	51	43	3
HOMO-1	2	94	1
HOMO-2	1	97	0
HOMO-3	4	92	1
HOMO-4	11	83	1
LUMO	87	11	4
LUMO+1	89	0	17
LUMO+2	45	0	51
LUMO+3	29	2	62
LUMO+4	24	6	60

The results obtained from the DOS analysis of all the molecules (SL1, SL2 and SL3) demonstrate that the donor and accepter fragments have comparable contributions. Specifically, the donor fragment exhibits a major contribution in the grand state, while the acceptor moieties dominate in the excited state [65]. This indicates strong conjugation and facilitates charge transfer from the donor to accepter fragments of the molecules, potentially enhancing the overall efficiency of compound. After analyzing the graph and FMCs of all designed molecules, their contribution to the development of HOMO LUMO energy level has been calculated [66]. In SL1 molecule fragment I shows less contribution for the formation of HOMO and LUMO as compared to fragment 2 which shows the maximum contribution. While the least percentage contribution shown by fragment 3. As the right side of the graph supports the contribution of the LUMO molecule. It is observed that fragment 3 is contributing only is the formation of LUMO energy levels and does not participate in the formation of HOMO [67]. While in the case of SL2 as the number of fragment 3 increases, its percentage contribution also increases almost equal to fragment 1 because fragment 3 doubled in number. While in the case of SL3 molecule fragment 3 contribution increases as compared to fragment 1 but fragment 2 still shows the maximum contribution for both HOMO and LUMO energy levels [68].

3.8. Transition Density Matrix Analysis

The utilization of Transition-Density of the matrix (TDMs) is highly regarded as a valuable technique to investigate and depict electronic transition processes. By providing a distinct three-dimensional map, TDMs allow for the determination of coherence lengths and delocalization pertaining to each electronic transition between two eigenstates of the developed molecule. TDMs are employed to elucidate charge-transfer excitations [69]. To analyze the emission and absorption of the developed compounds SL1, SL2, and SL3, as well as the reference compound SL, up to six excited states, the CAM-B3LYP/6-31G(d,p) level of theory is employed. This analysis is conducted using the Multiwfn3.8 software at the CAM-B3LYP/6-31G(d,p) /TD (n states=6) level of theory [70]. The significance of hydrogen has been underestimated due to its minimal contribution to electronic transitions. To investigate the electronic charge density of molecules using basis sets 6-31G(d,p) at the CAM-B3LYP level, the molecules are segmented into various components such as cores, acceptors, and bridge components. Figure 9 demonstrates the segmentation of these molecules into distinct segments (indicated by sequentially numbered atoms from 1 to the total number of atoms in the molecule) at the bottom, while the electron density is depicted on the left side of the y-axis [71].

Our TDM studies indicate that charge coherence is present in all compounds. Charge coherence is observed on the donor side of the reference compounds. Furthermore, charge coherence can be observed in donors and bridging units in SL1. Interestingly, SL1-SL2 molecules appear to exhibit greater coherence compared to SL1 [72]. Our analysis of electron coherence behavior in the developed molecules SL1-SL2 and the reference compound (R) reveals that charge coherence transitions from the donor to the bridging block. This bridging block facilitates electron transport without trapping them, ultimately leading to the transfer of charge density to the acceptor segment [73].

Based on our findings, electron coupling in all investigated compounds may be weaker than that of the reference compound, but exciton dissociation in the excited state could be more pronounced and straightforward. Binding energy serves as a useful method for assessing the performance of organic solar cells [74]. This approach involves the calculation of Coulombic interaction between electrons and holes within

the system. Compounds with low binding energy show Coulombic interactions between electrons and hole, while those have high binding energy display stronger interactions [75]. The binding energy value is defined as the difference between the HOMO-LUMO energy gap and the minimum excitation energy required for the first electron-hole excitation. This technique provides a valuable tool for evaluating the efficiency of molecules in scientific research. Equation can be used to compute the binding energy [76].

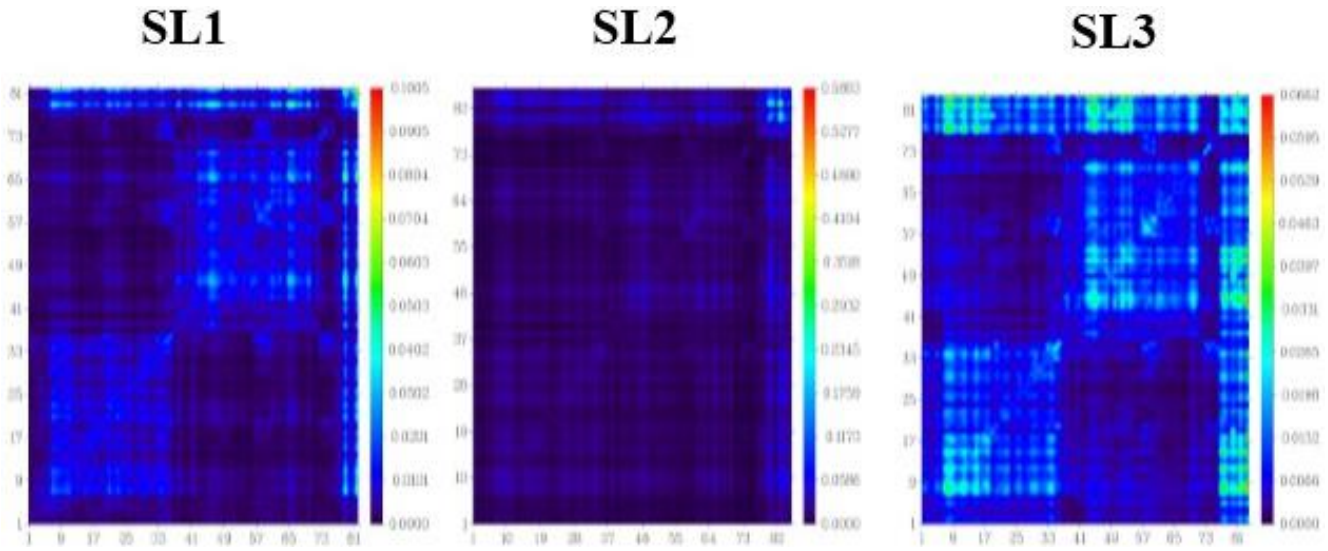

$$E_b = E_{H\text{-}L} - E_{opt}$$

Figure 9. *Two-dimensional graph illustrating the total density matrix (TDM) for the studied molecules (SL1, SL2, and SL3) is presented utilizing the DFT/CAM-Bee-3LYPmethod, with a specific emphasis on the A-D-A molecular configuration.*

3.9. Reduction Density Gradient Analysis

Reduced density gradient analysis is a theoretical tool used in computational science to learn nature of chemical bonding in a molecule. It provides information about the distribution of electron density and the strength of chemical interactions [77]. RDG is typically represented as a color-coded map, where different colors correspond to different types of interactions. RDG analysis is also emphasis to identify bond paths, bond critical points, and other features that provide insights into the behavior of bonding in the compounds [78]. RDG analysis, we can get meaningful information about nature of chemical bonding in the compounds, including the strengths of various interactions, such as covalent or non-covalent bonds, and the locations of bond critical points. RDG is a useful technique for understand the interaction in an investigated molecule such as intermolecular, intramolecular, dipole-dipole moment, Vander wall forces, hydrogen bonding, and covalent interaction [79]. The three different colors of the investigated molecule. Red coloure portion show the strong interaction, blue coloure portion represent the strong hydrogen bonding, and green coloure portion represent the Vander wall forces of the investigated molecules. This analysis can help in understanding the structure-activity relationship and reactivity of the Schiff base compounds [80].

In the Figure 10 SL1, SL2, and SL3, the 3D isosurface of 2-((ethylamine) methyl-6-methoxyphenol and 2D scatter plot shows the relationship between the reduced-density gradient and electron intensity (r), marked by λ2. The plot indicates that an I2 value where r = 0 corresponds to weak van der Waals forces [81]. When I2 at r is greater than zero, it indicates steric hindrance, while a negative value (+0.07 eV) denotes a weak hydrogen bond between the complex's constituent parts. A weak contact and hydrogen bond form between the N-atom of surface molecules and the OH-atom of the substituent, facilitating molecule release and binding to the intended site [82]. Non-covalent interactions between the carrier and drug are crucial for efficient drug delivery at the target area. Geometric optimization studies revealed a moderate correlation between the surface molecule and substituent group [83]. These weak interactions are beneficial as they allow for rapid drug unloading at the target site. The research indicates that the binding properties of SL1 and SL2 with the target molecules are greater than those of SL3. It was predicted that the presence of OH and Cl groups at the ortho position on the surface molecule enhances binding with the target molecules [84].

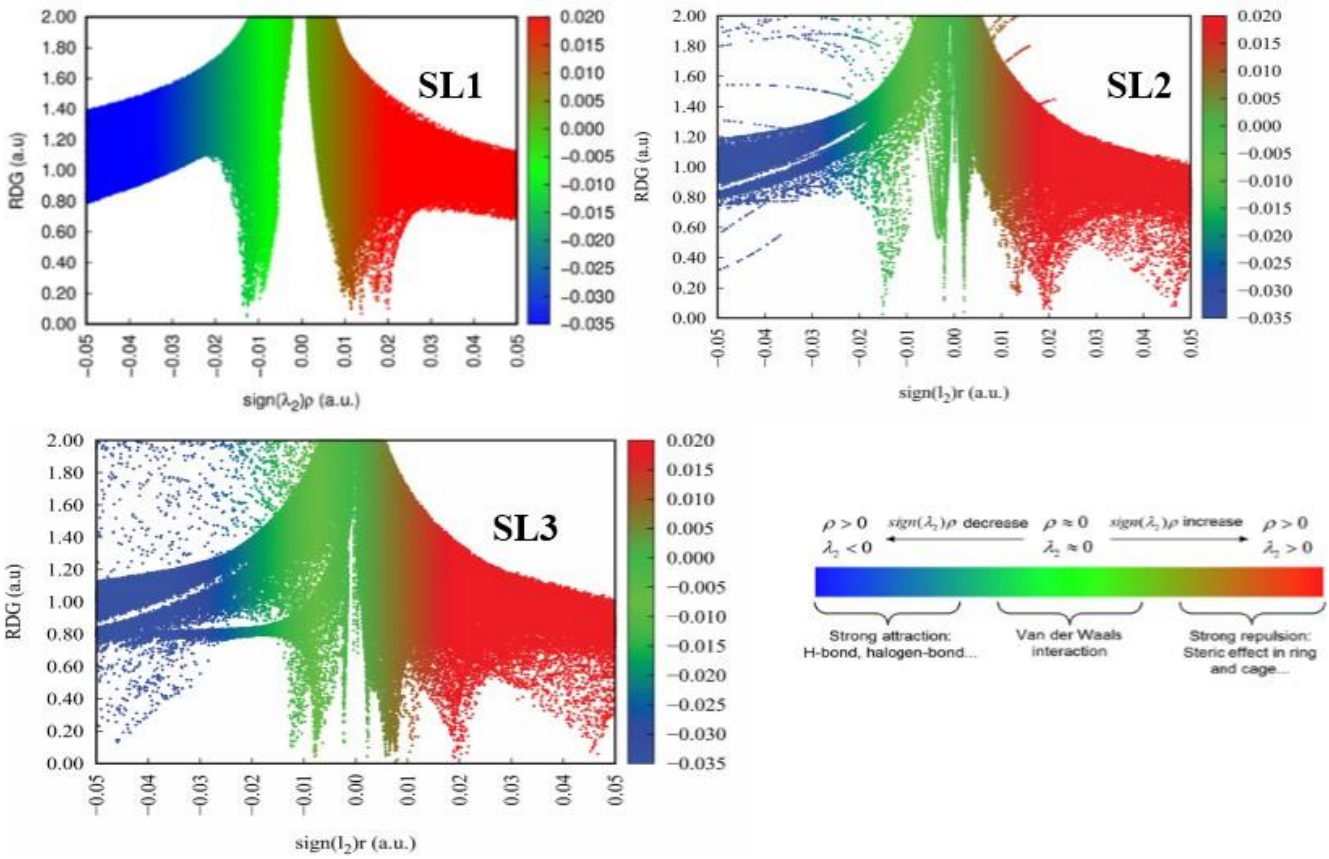

Figure 10. RDG values of SL1, SL2, and SL3.

3.10. Non Bonding Orbital Analysis

NBO analysis is a computational method used to understand the electronic structure and bonding interactions in molecules. It provides insights into the nature of chemical bonds, their strengths, and contributions from different orbitals [85]. These orbitals represent electronic shape and bonding forces within the molecule. NBO analysis can provide information about lone pairs, bonding orbitals, and delocalization of electrons, among other factors. It give help about the electronic determination and non-bonding in a molecules, helping to elucidate their properties and reactivity [86].

Table 7. NBO analysis.

Donor	Type	Acceptor	Type	E (1) Kcal mol^{-1}	E (J)-E (I) (a. u)	F (I, J) (a. u)
C24-C25	Π	C23-N7	π*	39.48	0.29	0.107
C17-C18	Π	C9-C10	π*	29.85	0.35	0.091
C15-C26	Π	C17-C18	π*	24.72	0.37	0.087
C8-N6	Π	C9-C10	π*	10.18	0.44	0.061
C12-C14	Π	C1-C2	σ *	2.52	0.92	0.047
C3-O1	Π	C18-O16	π*	0.93	0.53	0.021
C15-O2	Π	C15-O9	π*	0.55	0.56	0.016
C18-C19	Σ	C7-C8	σ *	3.98	1.43	0.068
C14-C18	Σ	C8-C4	σ *	3.88	1.34	0.064
C4-C31	Σ	C4-N5	σ *	3.41	1.36	0.061

Donor	Type	Acceptor	Type	E (1) Kcal mol^{-1}	E (J)-E (I) (a. u)	F (I, J) (a. u)
C24-H29	Σ	C25-C26	σ *	2.99	1.16	0.053
C13-C23	Σ	C10-C11	σ *	2.74	1.35	0.054
C17-C18	Σ	C18-C17	σ *	2.01	1.27	0.046
C15-C16	Σ	C16-C17	σ *	1.89	1.29	0.045
C1-C2	Σ	C1-N5	σ *	1.32	1.28	0.037
C17-H22	Σ	C17-C18	σ *	0.84	1.16	0.028
C9-H13	Σ	C8-C9	σ *	0.53	1.13	0.022
C7-O4	Σ	C17-O3	σ *	0.51	1.62	0.026
C26	LP(1)	C23-N2	π*	83.86	0.11	0.094
C9	LP(1)	C15-C18	π*	67.27	0.21	0.128
O5	LP(2)	C8-O1	π*	55.11	0.39	0.132
C18	LP(1)	C16-C17	π*	47.36	0.2	0.111
O3	LP(3)	C18-O4	π*	41.88	0.39	0.122
N2	LP(1)	C11-C13	π*	1.03	0.07	0.031
O3	LP(2)	C3-O4	π*	25.99	0.43	0.096
O4	LP(2)	C6-C7	σ *	20.65	0.8	0.119
O2	LP(2)	C7-O2	σ *	12.57	0.98	0.104
N2	LP(1)	C10-C11	σ *	8.26	0.99	0.082
N5	LP(1)	N2-H18	σ *	2.67	0.96	0.046
O1	LP(1)	C15-O7	σ *	1.72	1.4	0.044
N2	LP(1)	C11-C13	σ *	1.05	1.07	0.03
C8	LP(1)	C18-N9	σ *	0.52	0.63	0.022

Natural Bonding Orbital (NBO) analysis provides us a detailed insights into the electronic structure of molecules. This analysis give the huge information specifically, nature of bonding i.e bonding, anti-bonding, lone pair, bond pair, bond order, atomic charges, electronegativity, natural population i.e number of electrons contribution of each atom, delocalization Effects, hyper conjugation, resonance, and hybridization [87]. These orbitals are typically more chemically intuitive than canonical molecular orbitals. Bond Orders Quantifies the strength and character of bonds between atoms, including single, double, triple, and partial bonds. Atomic charges and electronegativity Natural Population Analysis (NPA) assigns electron densities to individual atoms, providing atomic charges that reflect the electron distribution in a molecule [88]. Electronegativity and chemical hardness. Hyper conjugation and Resonance Evaluates the extent of electron delocalization between bonding and anti-bonding orbitals or lone pairs, highlighting resonance structures and hyper conjugative interactions [89]. Lone Pairs and Core Orbitals Lone Pair Characterization Identifies and characterizes lone pairs on atoms, including their spatial distribution and interaction with other orbitals. Core orbitals provides information on the core orbitals that are typically less involved in chemical bonding but can still play a role in the overall electron density distribution [90]. Hybridization hybrid orbital analysis. Determines the hybridization state of atoms, describing how atomic orbitals mix to form bonding and lone pair orbitals. This helps in understanding the geometry and reactivity of the molecule. Stabilization energies second-order Perturbation Theory analysis estimates the stabilization energy due to interactions between filled (donor) and empty (acceptor) orbitals, providing insights into non-covalent interactions and intramolecular forces [91]. The NBO analysis examined both the filled orbitals and virtual orbital spaces, offering valuable insights for studying intramolecular and intermolecular interactions within the components of the investigated molecules [92]. Overall, NBO analysis provides a comprehensive picture of the electronic structure of molecules, aiding in the understanding of chemical bonding, molecular geometry, reactivity, and interaction mechanisms at a fundamental level show the investigated

molecules SL1, SL1, and SL3 have the different values of different characteristic [93]. SL1 molecule has highest electronegativity values due the presence of more electronegative atom oxygen than SL3 molecules has intermediated electronegativity values of due to Cl atom and SL3 has least electronegativity value. SL1 molecule compute high delocalization charger than SL1 and SL3 molecules due more resonance. SL1 also compute more natural population than SL2 has middle and SL3 has less natural population due to number atom are contribute (Table 7).

4. Summary

In this research work, we determined the spectroscopic, molecular, and electrostatic property of the designed Schiff base molecules SL1, SL2, and SL3 using GaussView5 and Gaussian 09. All designed and reference molecule were theoretically investigation utilization time-dependent density functional theory and density functional theory using B3LYP functional and a 6-31G(d,p) base set. Additionally, we analyzed the optical electronic and structure properties of the reference molecules (SL) after introducing different functional groups on the analytes molecules. We studied three functional groups OCH_3, CH_3, and Cl. Our calculations revealed that the OCH_3 functional group has a greater electron withdrawing effect compared to CH_3 and Cl. This research focused on molecules containing both electrons withdrawing and electrons donating groups. The spectroscopic and biological properties of the investigated molecules was compared with those of the reference molecules (SL). In our proposed scheme, we substituted the electron-withdrawing group in SL1 with another electron-withdrawing group, while electron-donating groups were substituted in SL2 and SL3. These substitutions resulted in decreased HOMO, LUMO, and energy gap values in the designed molecules, with SL3 showing the lowest energy gap of 2.82 eV and the broadest absorption spectra. Computational tools of the FMO revealed that the main transition in SL3 is characterized as a π-π* transition. Our results indicated that the distribution pattern of FMOs in the investigated molecules (SL1-SL3) affects the HOMO, LUMO, and energy gap values. After analyzing the simulated absorption spectra, we concluded that SL3 is red-shifted compared to the reference molecules (SL). These result show that designed molecules SL3 has the best results and is a suitable compound.

Abbreviations

DFT	Density Functional Theory
TD-DFT	Time dependent-Density Functional Theory
DOS	Density of State
TDM	Transition Density of Matrices
NBO	Natural Bod Orbital
VIE	Vertical Ionization Energy
EDDM	Electron Density Difference Map
FMOs	Frontier Molecular Orbitals
MEPs	Molecular Electrostatic Potentials

Acknowledgments

This research article was write by the author and co-authors without any external financial support. The draft of this work, including writing and graphic and designing, was carried out at the Department of Chemistry, University of Agriculture Faisalabad (38000), Punjab, Pakistan.

Author Contributions

Muhammad Javid: Conceptualization, Formal Analysis, Funding acquisition, Investigation, Project administration, Supervision, Validation, Writing – original draft

Ifra Shahzadi: Data curation, Formal Analysis, Investigation, Validation, Writing – review & editing

Farah Jamil: Investigation, Writing – review & editing

Sabahat Asghar: Formal Analysis, Investigation, Validation, Writing – original draft, Investigation

Muhammad Sajid Abbas: Conceptualization, Investigation, Writing – review & editing

Ihsan Maseeh: Formal Analysis, Funding acquisition, Validation

Muhammad Hasnain: Conceptualization, Supervision

Muhammad Zohaib Sabir: Investigation, Writing – original draft, Writing – review & editing

Conflicts of Interest

On behalf of all authors, the corresponding author states that there is no conflict of interest.

References

[1] Lasri, J., Eltayeb, N. E., Soliman, S. M., Ali, E. M., Alhayyani, S., & Akhdhar, A. (2023). Synthesis, crystal structure, DFT, and anticancer activity of some imine-type compounds via routine schiff base reaction: an example of unexpected cyclization to oxazine derivative. *Molecules*, *28*(12), 4766.

[2] Manvatkar, V. D., Patle, R. Y., Meshram, P. H., & Dongre, R. S. (2023). Azomethine-functionalized organic-inorganic framework: an overview. *Chemical Papers*, *77*(10), 5641-5662.

[3] Moanta, A. (2025). Classification, synthesis, isomerism, and spectral characterization of Schiff bases. *Mini-Reviews in Organic Chemistry*.

[4] Mushtaq, I., Ahmad, M., Saleem, M., & Ahmed, A. (2024). Pharmaceutical significance of Schiff bases: an overview. *Future Journal of Pharmaceutical Sciences*, *10*(1), 16.

[5] Islam, M. H., & Hannan, M. A. (2024). Schiff bases: contemporary synthesis, properties, and applications. In *Novelties in Schiff bases*. IntechOpen.

[6] Çınar, E. (2025). SCHIFF BASES: STRUCTURE, PROPERTIES AND APPLICATIONS. *From Molecule to Discipline: Contemporary and Innovative Approaches in Chemical Science*, 131.

[7] Mariam Abdul-Bary, M. A. B., Sweah, Z. J., & Sweah, Z. J. (2026). Schiff Bases and Their Complexities: A Review. *Schiff Bases and Their Complexities: A Review*, *3*(1), 26-48.

[8] TAŞ, N. A. (2024). AMINO ACID SCHIFF BASES: DEFINITION, PROPERTIES AND APPLICATIONS. *Modern Research and Investigations in Natural and Mathematical Sciences-II*, 75.

[9] Feng, H., Yang, P., Fu, J., Qin, M., & Zhang, K. (2025). Substituent-Engineered Multi-Stimuli-Responsive Schiff Base Crystals: from Proton Transfer Mechanisms to Smart Device Prototypes. *Crystal Growth & Design*, *25*(19), 8203-8216.

[10] Mandal, P., & Pratihar, J. L. (2023). A review of the photochromic behavior of metal complexes embedded in conjugated (-N= N-C= N-) and non-conjugated azo-imine-based ligands. *Reviews in Inorganic Chemistry*, *43*(4), 583-625.

[11] Li, D., Liang, X., Zhang, F., Li, J., Zhang, Z., Wang, S.,. & Guo, K. (2022). Imine bond orientation manipulates AIEgen derived Schiff base isomers through the intramolecular hydrogen bond effect for different fluorescence properties and applications. *Journal of Materials Chemistry C*, *10*(30), 11016-11026.

[12] Cossío, F. P., de Cózar, A., Sierra, M. A., Casarrubios, L., Muntaner, J. G., Banik, B. K., & Bandyopadhyay, D. (2022). Role of imine isomerization in the stereocontrol of the Staudinger reaction between ketenes and imines. *RSC advances*, *12*(1), 104-117.

[13] Khan, Y., Sarfraz, H., Rehman, W., Khan, M., Rasheed, L., & Rahman, K. U. (2025). Innovative horizons in drug design: exploring the synthesis and medicinal properties of heterocyclic schiff bases. A review. *Mini-Reviews in Medicinal Chemistry*, *25*(10), 727-744.

[14] Omar, I., Alharas, M. M., Feizi-Dehnayebi, M., Alharbi, S. K., Abo-Dief, H. M., Qasem, H. A.,. & Abu-Dief, A. M. (2025). Design, Synthesis, Physico-Chemical Characterization, Stability Determination, and Biomedical Applications of Some Novel Tetra-Dentate Imine Metal Chelates Supported by Theoretical Approaches: Bridging Coordination Chemistry and Life Sciences. *Applied Organometallic Chemistry*, *39*(3), e70056.

[15] Biswas, T., Mittal, R. K., Sharma, V., Kanupriya, & Mishra, I. (2024). Schiff bases: versatile mediators of medicinal and multifunctional advancements. *Letters in Organic Chemistry*, *21*(6), 505-519.

[16] Abdelsalam, M. M., Seadawy, M. G., Eldesouky, M., & El-Sherif, A. A. (2026). Comprehensive Thesis Review Structure: Schiff Bases in Modern Medicine and Biotechnology. *Egyptian Journal of Chemistry*.

[17] Abdel-Rahman, L. H., Al-Farhan, B. S., Nafady, A., Omar, I., Aljohani, F. S., Shehata, M. R., ... & Abu-Dief, A. M. (2025). Design, Preparation, Physicochemical Characterization, and DFT Calculations of Some Novel Complexes Based on Bi-Dentate Imine Ligand: Biomedical Applications and Molecular Docking Approach. *Applied Organometallic Chemistry*, *39*(3), e70052.

[18] Qian, C., Feng, L., Teo, W. L., Liu, J., Zhou, W., Wang, D., & Zhao, Y. (2022). Imine and imine-derived linkages in two-dimensional covalent organic frameworks. *Nature Reviews Chemistry*, *6*(12), 881-898.

[19] Rudolf, R., Neuman, N. I., Walter, R. R., Ringenberg, M. R., & Sarkar, B. (2022). Mesoionic Imines (MIIs): Strong Donors and Versatile Ligands for Transition Metals and Main Group Substrates. *Angewandte Chemie International Edition*, *61*(25), e202200653.

[20] Elangovan, N., Sowrirajan, S., Alzahrani, A. Y. A., Rajendran Nair, D. S., & Thomas, R. (2024). Fluorescent azomethine by the condensation of sulfadiazine and 4-chlorobenzaldehyde in solution: synthesis, characterization, solvent interactions, electronic structure, and biological activity prediction. *Polycyclic Aromatic Compounds*, *44*(4), 2332-2353.

[21] Bakr, E. A., Atteya, E. H., Al-Hefnawy, G. B., El-Attar, H. G., & El-Gamil, M. M. (2023). A novel azo-azomethine benzoxazole-based ligand and its transition metal (II), (III), (IV) complexes: Synthesis, characterization, theoretical studies, biological evaluation, and catalytic application. *Applied Organometallic Chemistry*, *37*(4), e7042.

[22] Dömötör, O., May, N. V., Gál, G. T., Spengler, G., Dobrova, A., Arion, V. B., & Enyedy, É. A. (2022). Solution Equilibrium Studies on Salicylidene Aminoguanidine Schiff Base Metal Complexes: Impact of the Hybridization with L-Proline on Stability, Redox Activity and Cytotoxicity. *Molecules*, *27*(7), 2044.

[23] Liu, Y., Bian, C., Li, Y., Sun, P., Xiao, Y., Xiao, X.,. & Dong, X. (2023). Aminobenzaldehyde convelently modified graphitic carbon nitride photocatalyst through Schiff base reaction: Regulating electronic structure and improving visible-light-driven photocatalytic activity for moxifloxacin degradation. *Journal of Colloid and Interface Science*, *630*, 867-878.

[24] Raczuk, E., Dmochowska, B., Samaszko-Fiertek, J., & Madaj, J. (2022). Different Schiff bases—structure, importance and classification. *Molecules*, *27*(3), 787.

[25] El Batouti, M., El-Mossalamy, E. H., & Elewa, M. M. (2026). Donor-acceptor dichotomy in novel Schiff bases: comprehensive spectroscopic and DFT investigation of intramolecular hydrogen bonding and charge-transfer properties. *RSC advances*, *16*(22), 19729-19742.

[26] Sánchez-Pacheco, A. D., Hernández-Vergara, M., Jaime-Adán, E., Hernández-Ortega, S., & Valdés-Martínez, J. (2021). Schiff bases as possible hydrogen bond donors and acceptors. *Journal of Molecular Structure*, *1234*, 130136.

[27] Nath, S., Bhattacharya, B., Sarkar, U., & Singh, T. S. (2022). Solvent effects on the photophysical properties of a donor-acceptor based Schiff base. *Journal of Fluorescence*, *32*(4), 1321-1336.

[28] Er-rajy, M., Salghi, R., Elhallaoui, M., Azzaoui, K., Chafiq, M., Elboughdiri, N.,. & Ko, Y. G. (2025). Exploring donor-acceptor characteristics and adsorption behavior of a naphthamide-based inhibitor for protective surfaces through a molecular modeling approach. *Journal of the Indian Chemical Society*, *102*(4), 101640.

[29] Lakhera, S., Rana, M., & Devlal, K. (2022). Theoretical study on spectral and optical properties of essential amino acids: a comparative study. *Optical and Quantum Electronics*, *54*(11), 714.

[30] Alkhatib, F. M., & Alsulami, H. M. (2023). Synthesis, characterization, DFT calculations and biological activity of new Schiff base complexes. *Heliyon*, *9*(8).

[31] Yavuz, Ş., Çolak, N., Yıldırım, T., Köse, D. A., & Şahin, O. (2026). Complexes formed by a heterocyclic schiff base containing an aminothiophene group with Ni (II) and Co (II) metals and their structural characterization. *Journal of Molecular Structure*, *1357*, 145217.

[32] Raju, S. K., Settu, A., Thiyagarajan, A., Rama, D., Sekar, P., & Kumar, S. (2022). Biological applications of Schiff bases: An overview. *GSC Biol. Pharm. Sci*, *21*(3), 203-215.

[33] Wang, L., & Yang, D. (2023). Take Advantage of the N-Nucleophilicity of Imine in Catalytic Cyclization Reactions. *ChemCatChem*, *15*(9), e202300189.

[34] Martínez, R. F., Matamoros, E., Cintas, P., & Palacios, J. C. (2020). Imine or Enamine? Insights and predictive guidelines from the electronic effect of substituents in H-bonded salicylimines. *The Journal of Organic Chemistry*, *85*(9), 5838-5862.

[35] Lv, H., Du, Y., Zhang, H., Zheng, Y., Yan, Z., & Dong, N. (2023). Advances in Mannich-type Reactions Based on the Classification of Compounds with Activated α-H. *ChemistrySelect*, *8*(21), e202300173.

[36] Guan, H., Sun, H., & Zhao, X. (2025). Application of density functional theory to molecular engineering of pharmaceutical formulations. *International journal of molecular sciences*, *26*(7), 3262.

[37] Tegegn, D. F., Belachew, H. Z., & Salau, A. O. (2024). DFT/TDDFT calculations of geometry optimization, electronic structure and spectral properties of clevudine and telbivudine for treatment of chronic hepatitis B. *Scientific Reports*, *14*(1), 8146.

[38] Napiórkowska, E., Milcarz, K., & Szeleszczuk, Ł. (2023). Review of applications of density functional theory (DFT) quantum mechanical calculations to study the high-pressure polymorphs of organic crystalline materials. *International Journal of Molecular Sciences*, *24*(18), 14155.

[39] Ahmed, L., & Omer, R. (2020). Population Analysis and UV-Vis spectra of Dopamine Molecule Using Gaussian 09. *Journal of Physical Chemistry and Functional Materials*, *3*(2), 48-58.

[40] Bálint, D., & Jäntschi, L. (2021). Comparison of molecular geometry optimization methods based on molecular descriptors. *Mathematics*, *9*(22), 2855.

[41] Kanagathara, N., & Nanmaran, R. (2021). Illustration of potential energy surface from DFT calculation along with fuzzy logic modelling for optimization of N-acetylglycine. *Computational and Theoretical Chemistry*, *1202*, 113301.

[42] Nkoe, P., Manicum, A. L. E., Louis, H., Malan, F. P., Nzondomyo, W. J., Chukwuemeka, K.,. & Unimuke, T. O. (2023). Influence of solvation on the spectral, molecular structure, and antileukemic activity of 1-benzyl-3-hydroxy-2-methylpyridin-4(1H)-one. *Journal of Molecular Liquids*, *370*, 121045.

[43] Limbu, S., Ojha, T., Ghimire, R. R., & Rai, K. B. (2024). An investigation of vibrational analysis, thermodynamics properties and electronic properties of Formaldehyde and its stretch by substituent acetone, acetyl chloride and methyl acetate using first principles analysis. *BIBECHANA*, *21*(1), 23-36.

[44] Gounhalli, S. G., Bhagyalaxmi, B., Konda, R. B., & Shivaleela, B. (2024). DFT Studies on Excited State Geometry, Vibrational Modes, NMR, Molecular Orbital and Mulliken Charges of Laser Dye. *Mapana Journal of Sciences*, *23*(4), 53.

[45] Wu, T., Fang, Z., Wang, Z., Liu, L. E., Song, J., & Song, J. (2023). Stability, electronic and catalytic properties of ConMoP (n= 1~ 5) clusters: A DFT study. *Journal of molecular modeling*, *29*(8), 269.

[46] Yildiz, E. A., Pepe, Y., Erdener, D., Karatay, A., Boyacioglu, B., Ünver, H.,. & Elmalı, A. (2023). Effect of group electronegativity on spectroscopic, biological, chromogenic sensing and optical properties of 2-formyl-benzene sulfonic acid sodium salt-based Schiff bases. *Journal of Molecular Structure*, *1286*, 135611.

[47] Li, L., Xu, S., Jin, L., Chen, W., & Chen, S. (2025). Efficient synergistic enhancing degradation of waste poly (ethylene terephthalate) by combination of DBU with zinc 2-ethylhexanoate. *Journal of Environmental Chemical Engineering*, *13*(3), 116308.

[48] Asrafali, S. P., Periyasamy, T., & Kim, S. C. (2023). Rapid transformation in wetting properties of PTFE membrane using plasma treatment. Polymers, 15(19), 3874.

[49] Kahraman, S., Hepokur, C., Erci, F., Erkan, S., Cetin, S., Kose, M., & Kurtoglu, M. (2025). Copper (II) complexes with N, O-donor azo-Schiff base ligands: Synthesis, structure, DFT studies, molecular docking, anticancer and antimicrobial activity. *Polyhedron*, *269*, 117393.

[50] Liao, G., Ruan, M., Wang, Y., Chen, H., & Weng, Y. (2025). IR fingerprint of the intermolecular hydrogen bond on amino acids and its relevance to chaperone activity of αB-crystallin. The Journal of Physical Chemistry B, 129(4), 1237-1247.

[51] Xiao, P., Liu, S., Zhou, X., Huang, E., Zhong, L., Zhang, W.,. & Dong, W. (2024). Structure and vibrational spectroscopy of 2-methylallyl alcohol. Chinese Journal of Chemical Physics, 37(4), 481-489.

[52] Ali, H. F., Adeel, M., Aiman, U., Jamal, S., Haroon, M., & Ahamad, T. (2025). Synthesis, spectral characterization and nonlinear optical exploration of potent fluorene-based compounds: A DFT refine experimental study. Journal of Molecular Structure, 143630.

[53] Shafiq, I., Irshad, I., Zahid, R., Mahmood, K., Ahmed, S., Bullo, S., & Alhokbany, N. (2025). Exploration of promising key electronic and nonlinear optical properties of bifluorenylidene based chromophores: a TD-DFT/DFT approach. Scientific Reports, 15(1), 10701.

[54] Khalid, M., Khan, M., Gull, K., Mubarak, M., Arshad, M. N., & Imran, M. (2026). Exploring the NLO potential of new designed thieno[2]indole-based derivatives via donor group modification: a DFT study on static and frequency-dependent NLO properties. Journal of Computational Electronics, 25(1), 46.

[55] Lu, T. (2025). Visualization analysis of covalent and noncovalent interactions in real space. Angewandte Chemie International Edition, 64(29), e202504895.

[56] Lu, T. (2024). A comprehensive electron wavefunction analysis toolbox for chemists, Multiwfn. The Journal of chemical physics, 161(8).

[57] Marimuthu, M., Balasubramanian, S., Viswanathan, R. B., Parthiban, H. P., Mahalingam, M., & Kasirajan, G. (2025). An in-silico investigation of 8-hydroxyquinoline (8-HoQ) derivatives as potential anti-tuberculosis agents by targeting glutamate kinase. Structural Chemistry, 1-21.

[58] Warburton, R. E., Soudackov, A. V., & Hammes-Schiffer, S. (2022). Theoretical modeling of electrochemical proton-coupled electron transfer. Chemical reviews, 122(12), 10599-10650.

[59] Fichthorn, K. A., *Theory of anisotropic metal nanostructures.* Chemical Reviews, 2023. 123(7): p. 4146-4183.

[60] Sangari, S., Lackmy-Vallee, A., Preuilh, A., Peyre, I., Pradat, P. F., & Marchand-Pauvert, V. (2024). Synaptic dynamics linked to widespread elevation of H-reflex before peripheral denervation in amyotrophic lateral sclerosis. Journal of Neurophysiology, 132(5), 1541-1560.

[61] Allison, D., & Wong, M. (2026). Posterior Fossa. In Operative Neurophysiology: Practical Application for Comprehensive Neuromonitoring and Neuromapping Techniques (pp. 431-466). Cham: Springer Nature Switzerland.

[62] Toriyama, M. Y., Ganose, A. M., Dylla, M., Anand, S., Park, J., Brod, M. K.,. & Snyder, G. J. (2022). How to analyse a density of states. Materials today electronics, 1, 100002.

[63] Fung, V., Hu, G., Ganesh, P., & Sumpter, B. G. (2021). Machine learned features from density of states for accurate adsorption energy prediction. Nature communications, 12(1), 88.

[64] Sun, H. (2024). Unraveling the structure-property relationship of novel thiophene and furan-fused cyclopentadienyl chromophores for nonlinear optical applications. Journal of Computational Chemistry, 45(31), 2612-2623.

[65] UrRehman, S., Anwer, M., BiBi, S., Jamil, S., Yasin, M., Khan, S. R.,. & Jia, R. (2022). DFT analysis of different substitutions on optoelectronic properties of carbazole-based small acceptor materials for Organic Photovoltaics. Materials Science in Semiconductor Processing, 140, 106381.

[66] Contreras, P., Seijas, L., & Osorio, D. (2021). TDOS quantum mechanical visual analysis for single molecules. arXiv preprint arXiv: 2105.12830.

[67] Louis, H., Ifediora, L. P., Enudi, O. C., Unimuke, T. O., Asogwa, F. C., & Moshood, Y. L. (2021). Evaluation of the excited state dynamics, photophysical properties, and the influence of donor substitution in a donor-π-acceptor system. Journal of molecular modeling, 27(10), 284.

[68] Ziadi, K., Aouragh, A., & Messaoudi, A. (2025). Structure-property analysis of dithienopyrrole-based D-π-A-π-D compounds: electronic and nonlinear optical responses with advanced python-based visualizations. Journal of Molecular Graphics and Modelling, 140, 109113.

[69] Jamal, S., Raza, N., Khalid, M., & Braga, A. A. C. (2025). Unveiling electronic and remarkable non-linear optical properties of boron-nitrogen carbazole-based compounds via modification of π-linker and donor units: a DFT study. RSC advances, 15(11), 8262-8274.

[70] Li, N., Zhang, L., & Wang, J. (2023). Modulation of chiral spectral deflection by van der Waals force-induced molecular electropolarization in catenane oligomers. RSC advances, 13(16), 11055-11061.

[71] Khalid, M., Ahmed, R., Shafiq, I., Arshad, M., Asghar, M. A., Munawar, K. S.,. & Braga, A. A. (2022). First theoretical framework for highly efficient photovoltaic parameters by structural modification with benzothiophene-incorporated acceptors in dithiophene based chromophores. Scientific Reports, 12(1), 20148.

[72] Ren, Y., Gai, X., Wang, J., & Wang, L. (2025). Physical mechanism of nonlinear optical properties in Lemniscular carbon nanohoops. Chemical Physics, 593, 112655.

[73] Al-Matar, H. M., BinSabt, M. H., & Shalaby, M. A. (2025). Synthesis, Photophysical, and computational investigation of poly substituted pyridines. Journal of Molecular Structure, 143298.

[74] Sultan, N., Ikreedeegh, R. R., & Janjua, M. R. S. A. (2026). Review and Insights into the Impact of Transition Density Matrix (TDM) on the Optoelectronic Properties of Organic Solar Cells (OSCs). High Energy Chemistry, 60(1), 1-15.

[75] Aldawsari, F. S., Albugami, F. S., Altalhi, T. A., Refat, M. S., Shakya, S., Adam, A. M. A.,. & Jaber Altalhi, A. A. (2025). SPECTROSCOPIC MEASUREMENTS, COMPUTATIONAL CALCULATIONS, AND DRUG ASSAY APPLICATIONS OF CHARGE-TRANSFER COMPLEXES COMPRISING THE PHARMACEUTICAL TRIAMTERENE AND THE ORGANIC ACCEPTORS TCNQ AND DDQ. Bulletin of the Chemical Society of Ethiopia, 39(10).

[76] Shafiq, I., Khalid, M., Asghar, M. A., Baby, R., Braga, A. A., Alshehri, S. M., & Ahmed, S. (2023). Influence of azacycle donor moieties on the photovoltaic properties of benzo [c, 1, 2, 5] thiadiazole based organic systems: a DFT study. Scientific Reports, 13(1), 14630.

[77] Laplaza, R., Peccati, F., A. Boto, R., Quan, C., Carbone, A., Piquemal, J. P.,. & Contreras-García, J. (2021). NCIPLOT and the analysis of noncovalent interactions using the reduced density gradient. Wiley Interdisciplinary Reviews: Computational Molecular Science, 11(2), e1497.

[78] Morales-Pumarino, D., & Barquera-Lozada, J. E. (2023). Electron density and its reduced density gradient in the study of π-π interactions. International Journal of Quantum Chemistry, 123(18), e27051.

[79] Guerra, C., Burgos, J., Ayarde-Henríquez, L., & Chamorro, E. (2024). Formulating reduced density gradient approaches for noncovalent interactions. The Journal of Physical Chemistry A, 128(30), 6158-6166.

[80] Zhang, H., Liu, S., You, J., Liu, C., Zheng, S., Lu, Z.,. & Shao, B. (2024). Overcoming the barrier of orbital-free density functional theory for molecular systems using deep learning. Nature Computational Science, 4(3), 210-223.

[81] Lu, T., & Chen, Q. (2022). Independent gradient model based on Hirshfeld partition: A new method for visual study of interactions in chemical systems. Journal of computational chemistry, 43(8), 539-555.

[82] Kalita, B., Li, L., McCarty, R. J., & Burke, K. (2021). Learning to approximate density functionals. Accounts of Chemical Research, 54(4), 818-826.

[83] Li Manni, G., Fdez. Galván, I., Alavi, A., Aleotti, F., Aquilante, F., Autschbach, J.,. & Lindh, R. (2023). The OpenMolcas Web: A community-driven approach to advancing computational chemistry. Journal of Chemical Theory and Computation, 19(20), 6933-6991.

[84] Choudhary, K., DeCost, B., Chen, C., Jain, A., Tavazza, F., Cohn, R.,. & Wolverton, C. (2022). Recent advances and applications of deep learning methods in materials science. npj Computational Materials, 8(1), 59.

[85] Agwupuye, J. A., Louis, H., Unimuke, T. O., David, P., Ubana, E. I., & Moshood, Y. L. (2021). Electronic structure investigation of the stability, reactivity, NBO analysis, thermodynamics, and the nature of the interactions in methyl-substituted imidazolium-based ionic liquids. Journal of Molecular Liquids, 337, 116458.

[86] Jawad, H. M., & Jasim, F. A. (2024, May). Theoretical investigations on the natural bond orbital, HOMO-LUMO, contour maps, and energy gap of diatrizoate. In AIP conference proceedings (Vol. 3097, No. 1, p. 090004). AIP Publishing LLC.

[87] Santos-Jr, C. V., Kraka, E., & Moura Jr, R. T. (2025). Chemical bond overlap descriptors from multiconfiguration wavefunctions. *Journal of Computational Chemistry*, *46*(1), e27534.

[88] Edache, E. I., Uzairu, A., Mamza, P. A., Shallangwa, G. A., & Ibrahim, M. T. (2024). DFT studies on structure, electronics, bonding nature, NBO analysis, thermodynamic properties, molecular docking, and MM-GBSA evaluation of 4-methyl-3- [2-(4-nitrophenyl)-1, 3-dioxo-2, 3-dihydro-1 H-isoindole-5-amido] benzoic acid: a potent inhibitor of Graves' disease. Journal of Umm Al-Qura University for Applied Sciences, 10(4), 652-670.

[89] Miller, S. A. (2023). The location of the chemical bond. Application of long covalent bond theory to the structure of silica. Frontiers in chemistry, 11, 1123322.

[90] Weinhold, F. (2023). "Noncovalent interaction": A chemical misnomer that inhibits proper understanding of hydrogen bonding, rotation barriers, and other topics. Molecules, 28(9), 3776.

[91] Prabakaran, A., Maheswari, C. U., Issaoui, N., Al-Dossary, O. M., Rajamani, T., Gnanasambandan, T.,. & Manikandan, A. (2024). Computational insight into the spectroscopic and molecular docking analysis of estrogen receptor with ligand 2, 3-dimethyl-N [2-(hydroxy) benzylidene] aniline. Journal of King Saud University-Science, 36(6), 103196.

[92] Shiny, C. L., Rathika, A., Tarika, J. D., Alen, S., & Beaula, T. J. (2023). Effect of charge transfer and non-covalent interactions of the synthesized NLO compound p-nitrophenol sodium-bisulfate using DFT method. Polycyclic Aromatic Compounds, 43(5), 4621-4639.

[93] Medimagh, M., Issaoui, N., Gatfaoui, S., Kazachenko, A. S., Al-Dossary, O. M., Kumar, N.,. & Bousiakoug, L. G. (2023). Investigations on the non-covalent interactions, drug-likeness, molecular docking and chemical properties of 1, 1, 4, 7, 7-pentamethyldiethylenetriammonium trinitrate by density-functional theory. Journal of King Saud University-Science, 35(4), 102645.